sustainability

Article

Microgrid Robust Planning Model and Its Modification Strategy Based on Improved Grey Relational Theory

Jiayin Xu [1], Xu Gui [1], Kun Li [1], Guifen Jiang [1], Tao Wang [1] and Zhen Xu [2,*]

1 Economic and Technology Research Institute of State Grid Anhui Electric Power Co., Ltd., Hefei 230022, China
2 School of Electrical Engineering and Automation, Hefei University of Technology, Hefei 230009, China
* Correspondence: xu_zhen_yx@163.com

Abstract: A two-stage robust planning model is constructed in this paper, which can reduce the joint planning uncertainty of a wind-photovoltaic-energy storage system caused by the stochastic characteristics of renewable energy and ensure the sustainability of the power grid. Considering the life loss of energy storage system comprehensively, the joint planning is realized in the worst scenario. Addressing the problem that subjective and uniform robustness parameters in robust optimization cannot cope with the differentiated characteristics of each uncertainty, a robust microgrid-planning model and its modification strategy based on improved grey relational theory are proposed. The idea of weight distribution and dynamic value of identification coefficients are introduced into grey relational theory, so as to enhance the weight of indicators that influence planning and the relational degree between them, which can avoid the locally relational tendency. According to the relation degree, the renewable energy's robustness parameters are modified to improve the applicability and flexibility of the microgrid-planning results. Finally, the effectiveness and superiority of the proposed theory and method are verified using a case study approach.

Keywords: microgrid planning; renewable energy; robust optimization; grey relational theory; modification strategy

Citation: Xu, J.; Gui, X.; Li, K.; Jiang, G.; Wang, T.; Xu, Z. Microgrid Robust Planning Model and Its Modification Strategy Based on Improved Grey Relational Theory. *Sustainability* **2023**, *15*, 2835. https://doi.org/10.3390/su15032835

Academic Editors: Qian Xiao, Yiqi Liu, Jun Zeng and Fei Gao

Received: 12 December 2022
Revised: 29 January 2023
Accepted: 31 January 2023
Published: 3 February 2023

1. Introduction

The distributed renewable energy connected microgrid, which is represented by wind power and photovoltaic (PV), has been developed rapidly [1,2]. The microgrid planning model has become the research focus, combined with the joint planning for robustness of the wind-PV-energy storage system (ESS), because the optimal planning scheme is very important for the economic and sustainability of the power grid [3,4]. Most researchers focus on the planning model's setting and solving methods, such as the speed of the solving method and the applicability of the optimal scheme, but the adjustment effect of planning elements on the optimal solution is ignored. This paper proposes a microgrid robust planning model and its modification strategy to reduce the planning cost, based on improved grey relational analysis (IGRA) and the relational degrees among planning elements.

Based on the stochastic characteristics of renewable energy, the joint planning with the robustness of wind-PV-ESS is typically uncertain. The robust optimization (RO) algorithm has been widely used in solving the above problem because it is a method used to find certain robustness for optimization problems in uncertain environments and only requires the boundary of the uncertainty set [5–8]. Ref. [9] defines the boundary of the uncertainty set as a "robust parameter". To solve the planning scheme more efficiently and economically, Ref. [10] proposes the distributionally robust optimization (DRO) theory, which is an optimization method based on insufficient information and combines the solvability of RO and flexibility of stochastic programming. Refs. [11,12] use Wasserstein Distance to construct the fuzzy set for the probability distribution of renewable energy. Ref. [13]

uses matrix information to describe the probability distribution set of renewable energy's prediction errors. Ref. [14] proposes an indeterminately distributional model so that the probability distribution of uncertainties changes around a given reference range. All the above papers focus on the improvement of the algorithms' solving power and the planning model's setting to get the optimal solution. However, in these papers, the boundary of the uncertainty set does not consider the adjustment effect of uncertainty's property on the optimal solution. In this paper, a two-stage robust planning model is constructed, and uncertainties are represented by bounded closed-box uncertain sets which will be modified to reduce the planning cost innovatively.

Grey relational analysis (GRA) shows the hidden relation between indicators according to the similarity degrees of the geometric curves [15,16]. According to GRA, grey data refers to data with randomly variable characteristics, and grey system refers to the system that contains grey data [17,18]. In particular, the relational degree between grey data can reflect the changing characteristics of the grey system; as for the planning model, renewable energy can be seen as grey data, and the microgrid planning can be seen as a grey system. However, GRA adopts equal treatment for each analysis index, which biases the relational degree with discrete indexes and hides the characteristics of the indexes [19]. To solve the above problem, Ref. [20] redistribute the weights of the analyzed data based on their importance to the indicators. Ref. [21] combines the analytic hierarchy process with Delphi (AHPD) and GRA method to weight the grey data. Ref. [22] introduces the triangle fuzzy theory (TF), then Fuzzy-Grey Relational Analysis (F-GRA) is used to weight the grey data. Ref. [23] constructs the relative area change that reflects the similitude degree of the sequence curves, to define the new relational coefficient. Ref. [24] combines the entropy weight method (EWM) and analytic hierarchy process (AHP) to carry out combined weighting of grey relational degree. In this paper, IGRA is proposed based on weighting and using the dynamic value of identification coefficient innovatively; particularly, the identification coefficient of dynamic value is set up with TF.

This paper proposes a microgrid robust planning model and its modification strategy based on IGRA. Firstly, a two-stage robust planning model is constructed, which considers the life loss of the energy storage system and realizes the joint planning to ensure the robustness of wind-PV-ESS. Then, the planning model is solved in detail, by using Karush–Kuhn–Tucker (KKT) method and Column-and-Constraint Generation (C&CG) algorithm. Secondly, the idea of weight allocation and Triangle-shape grade of membership function is integrated into GRA, and then, IGRA is proposed with the dynamic value of identification coefficient to calculate the relational degrees between the robust microgrid-planning model's elements. Thirdly, the steps of modifying the robust planning model's robustness parameters are detailed with the obtained relational degrees. Finally, the feasibility and effectiveness of the proposed method are verified with a real microgrid system of a province in China.

2. Two-Stage Robust Planning for Microgrid

The microgrid-planning model includes a wind turbine (WT), PV, microturbine (MT), and ESS. For this, the uncertainty sets of renewable energy output and demand-side load, as well as the life model of ESS are constructed. Based on the above mathematical models, the objective function with the minimum total cost is proposed, including the initial investment costs and the operation costs, with the constraints of power balance, and the upper and lower limits of line power, generator outputs, the state of charge (SOC), and storage charging and discharging power. The microgrid-planning model of this paper is shown in Figure 1.

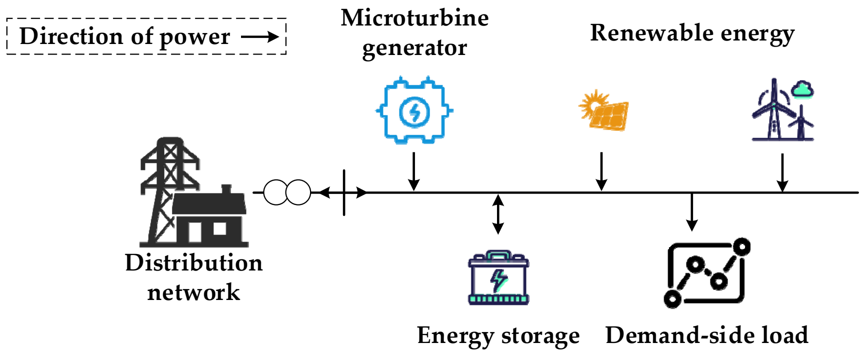

Figure 1. Microgrid-planning model of this paper.

2.1. Mathematical Model of the Microgrid Planning

2.1.1. Uncertainty Sets of Renewable Energy and Demand-Side Load

In the robust model of microgrid planning, the output of WT, PV and the demand-side load are uncertain (have uncertainties). The bounded closed-box uncertain sets U are used to express the range of these uncertainties, as shown in Equations (1)–(3). To effectively adjust the applicability of the planning schemes, the robust adjustment parameters, Γ_{wt}, Γ_{pv} and Γ_{load}, are introduced to represent the volatility of the above uncertainties.

$$U_{\mathrm{wt}} = \left\{ P_{\mathrm{wt},t} \in R^{NW \times T} : \sum_{t=1}^{T} \left| \frac{\Delta P_{\mathrm{wt},t}}{\Delta P_{\mathrm{wt},t}^{\max}} \right| \leq \Gamma_{\mathrm{wt}}, P_{\mathrm{wt},t} = P_{\mathrm{wt},t}^{0} + \Delta P_{\mathrm{wt},t} \right\} \tag{1}$$

$$U_{\mathrm{pv}} = \left\{ P_{\mathrm{pv},t} \in R^{NW \times T} : \sum_{t=1}^{T} \left| \frac{\Delta P_{\mathrm{pv},t}}{\Delta P_{\mathrm{pv},t}^{\max}} \right| \leq \Gamma_{\mathrm{pv}}, P_{\mathrm{pv},t} = P_{\mathrm{pv},t}^{0} + \Delta P_{\mathrm{pv},t} \right\} \tag{2}$$

$$U_{\mathrm{load}} = \left\{ P_{\mathrm{load},t} \in R^{NW \times T} : \sum_{t=1}^{T} \left| \frac{\Delta P_{\mathrm{load},t}}{\Delta P_{\mathrm{load},t}^{\max}} \right| \leq \Gamma_{\mathrm{load}}, P_{\mathrm{load},t} = P_{\mathrm{load},t}^{0} + \Delta P_{\mathrm{load},t} \right\} \tag{3}$$

where $P_{\mathrm{wt},t}^{0}$, $P_{\mathrm{pv},t}^{0}$ and $P_{\mathrm{load},t}^{0}$ are the predicted value of WT output and PV output, as well as the demand-side load respectively, during period t. $P_{\mathrm{wt},t}$, $P_{\mathrm{pv},t}$ and $P_{\mathrm{load},t}$ are the actual output values of WT and PV, as well as the demand-side load value. $\Delta P_{\mathrm{wt},t}^{\max}$, $\Delta P_{\mathrm{pv},t}^{\max}$ and $\Delta P_{\mathrm{load},t}^{\max}$ are the maximum fluctuation values of WT, PV and demand-side load, respectively.

To ensure the stable operation of the microgrid system, the fluctuation range of the above uncertainties is constrained, as shown in Equation (4).

$$\begin{cases} P_{\mathrm{wt},t}^{0} - \Delta P_{\mathrm{wt},t}^{\max} \leq P_{\mathrm{wt},t} \leq P_{\mathrm{wt},t}^{0} + \Delta P_{\mathrm{wt},t}^{\max} \\ P_{\mathrm{pv},t}^{0} - \Delta P_{\mathrm{pv},t}^{\max} \leq P_{\mathrm{pv},t} \leq P_{\mathrm{pv},t}^{0} + \Delta P_{\mathrm{pv},t}^{\max} \\ P_{\mathrm{load},t}^{0} - \Delta P_{\mathrm{load},t}^{\max} \leq P_{\mathrm{load},t} \leq P_{\mathrm{load},t}^{0} + \Delta P_{\mathrm{load},t}^{\max} \end{cases} \tag{4}$$

2.1.2. Life Model of ESS and Its Linearization

(1) Life model of ESS

In this paper, the battery is set as the ESS and to be only in a charging or discharging state during operation. The SOC of ESS is shown in Equation (5).

$$SOC_t = SOC_{t-1} + \left[\frac{\chi_{\mathrm{bat},t} \cdot P_{\mathrm{bat},t}^{\mathrm{ch}} \cdot \eta_{\mathrm{ch}}}{E_{\mathrm{bat}}^{\max}} - \frac{(1 - \chi_{\mathrm{bat},t}) P_{\mathrm{bat},t}^{\mathrm{dis}}}{E_{\mathrm{bat}}^{\max} \cdot \eta_{\mathrm{dis}}} \right] \Delta t \times 100\% \tag{5}$$

where SOC_t and SOC_{t-1} are the SOC during period t and period $(t-1)$, respectively. $P_{\mathrm{bat},t}^{\mathrm{ch}}$ and $P_{\mathrm{bat},t}^{\mathrm{dis}}$ are the charging and discharging power of the ESS, respectively. η_{ch} and η_{dis} are charging and discharging efficiency of the ESS, respectively, and they are usually set to

0.95 [25,26]. $E_{\text{bat}}^{\max}$s the rated capacity of the ESS. $\chi_{\text{bat},t}$ is a binary variable, whose value is 1 indicating that the battery is charged.

The depth of each charging and discharging cycle is the key factor affecting the service life of a battery. If this factor is ignored, the planning results tend to be optimistic [27]. The relationship between the discharge depth and the life of a battery is shown in Equation (6). Firstly, the cycle-discharging depth is determined by the rain-flow counting method; then, the cycle life can be fitted by the power function.

$$N_{\text{life}} = N_0 (D_{dod}^{\text{cyc}})^{-k_p} \tag{6}$$

where N_{life} is the number of cycles when the battery reaches the upper limit of its life. $D_{\text{dod}}^{\text{cyc}}$ is the discharging depth of the battery. N_0 is the number of cycles with which the battery can reach the life limit when it works at 100% discharging depth. k_p is the fitting coefficient of the power function.

However, Equation (6) is highly nonlinear and difficult to solve in the planning model, and the planning result is too conservative because Equation (6) replaces the maximum discharging depth with the current discharge depth of the ESS.

To solve the above problem, we simplify the problem into a life model based on the equivalent number for the cycle-discharging depth. Firstly, it is assumed that the battery has a charging and discharging cycle during period t, and its cycle-discharging depth is the discharging depth of the battery during the period ($t - 1$), as shown in Equations (7) and (8).

$$DOD_{t-1} = 1 - SOC_{t-1} \tag{7}$$

$$DOD_t^{\text{cyc}} = DOD_{t-1} \cdot \chi_{\text{SOC},t} \tag{8}$$

where DOD_{t-1} is the discharging depth during period ($t - 1$). DOD_t^{cyc} is the cycle-discharging depth. $\chi_{\text{SOC},t}$ is a binary variable, whose value is 1 indicating that the battery has a charging or discharging cycle.

Then, the moment of transformation of the charging and discharging state is determined by Equation (9).

$$\chi_{\text{bat},t} = \max\{\chi_{\text{SOC},t} - \chi_{\text{SOC},t-1}, 0\} \tag{9}$$

(2) Linearization of the life model

Firstly, based on the piecewise linearization of discharging depth completed above, the discharging depth can be divided into D segments. Constraint conditions are set to ensure that the ESS is only in a discharging or charging state at the dth discharging depth, as shown in Equations (10) and (11).

$$\sum_{d=1}^{D} \chi_{\text{SOC},t}^{d} = 1 \tag{10}$$

$$DOD_t^{d,\min} \chi_{\text{SOC},t}^{d} \le DOD_t^{d} \le DOD_t^{d,\max} \chi_{\text{SOC},t}^{d} \tag{11}$$

where $\chi_{\text{SOC},t}^{d}$ represents the charging or discharging state for d. $DOD_t^{d,\min}$ and $DOD_t^{d,\max}$ represent the lower and upper limits of the dth discharging depth, respectively.

Then, Equation (9) is determined by the Max function, and its equivalent linear form is shown in Equations (12)–(14).

$$\chi_{\text{SOC},t} - \chi_{\text{SOC},t-1} \le \chi_{\text{bat},t} \tag{12}$$

$$\chi_{\text{bat},t} \le \chi_{\text{SOC},t} \tag{13}$$

$$\chi_{\text{bat},t} \le 1 - \chi_{\text{SOC},t-1} \tag{14}$$

2.1.3. Model of Microturbine

The controllable power supply in micro grid mainly includes the MT, fuel cell and so on [28]. As for the MT, its response speed is faster in hour-level scheduling, which allows it to work better with ESS in a microgrid system; its climbing constraint can be ignored and only its output constraint is considered in this paper [9].

$$P_{\mathrm{G}}^{\min} \leq P_{\mathrm{G},t} \leq P_{\mathrm{G}}^{\max} \tag{15}$$

where $P_{\mathrm{G}}^{\min}$ is the minimum output of the MT.

2.2. Constraints of the Microgrid Planning

To ensure the stable operation of the planned microgrid, the constraints of the microgrid planning are as below, and include power balance, the upper and lower limits of line power, unit outputs, SOC, as well as storage charging and discharging power.

2.2.1. Constraints on Power Balance

In the microgrid planning, this constraint ensures the power supply and demand balance.

$$P_{\mathrm{wt},t} + P_{\mathrm{pv},t} + P_{\mathrm{bat},t}^{\mathrm{dis}} + P_{\mathrm{M},t}^{\mathrm{buy}} + P_{\mathrm{G},t} = P_{\mathrm{load},t} + P_{M,t}^{\mathrm{sell}} + P_{\mathrm{bat},t}^{\mathrm{ch}} \tag{16}$$

where $P_{\mathrm{G},t}$ is the real-time output of MT during period t. $P_{\mathrm{M},t}^{\mathrm{buy}}$ and $P_{\mathrm{M},t}^{\mathrm{sell}}$ are the power purchase and sale between microgrid and power grid during period t, respectively.

2.2.2. Constraints of the Generator Output

The response speed of the MT is faster in hour-level scheduling, so its climbing constraint can be ignored, and only its output constraint is considered in this paper.

$$P_{\mathrm{wt}}^{\min} \leq P_{\mathrm{wt},t} \leq P_{\mathrm{wt}}^{\max} \tag{17}$$

$$P_{\mathrm{pv}}^{\min} \leq P_{\mathrm{pv},t} \leq P_{\mathrm{pv}}^{\max} \tag{18}$$

where $P_{\mathrm{wt}}^{\min}$ and $P_{\mathrm{wt}}^{\max}$ are the lower and upper limits of WT, respectively. $P_{\mathrm{pv}}^{\min}$ and $P_{\mathrm{pv}}^{\max}$ are the lower and upper limits of PV, respectively.

2.2.3. Constraints of ESS

The constraints of ESS are constructed in this part, including the upper and lower limits of SOC and operating power, respectively.

(1) Constraints on the operating power

$$0 \leq P_{\mathrm{bat},t}^{\mathrm{ch}} \leq \chi_{\mathrm{bat},t}\varepsilon_{\mathrm{ch}}E_{\mathrm{bat}}^{\max} \tag{19}$$

$$0 \leq P_{\mathrm{bat},t}^{\mathrm{dis}} \leq (1-\chi_{\mathrm{bat},t})\varepsilon_{\mathrm{dis}}E_{\mathrm{bat}}^{\max} \tag{20}$$

where $\varepsilon_{\mathrm{ch}}$ and $\varepsilon_{\mathrm{dis}}$ are the ratios of the maximum charging and discharging power to the maximum capacity of the ESS, respectively.

(2) Constraints on the SOC

$$SOC^{\min} \leq SOC_t \leq SOC^{\max} \tag{21}$$

where $SOC^{\min}$ and $SOC^{\max}$ are the lower and upper limits of the SOC, respectively; they can avoid excessive charging and discharging of ESS. As shown in [29–31], $SOC^{\min}$ is generally set to 0.1–0.2, and $SOC^{\max}$ is generally set to 0.8–0.9.

2.2.4. Constraints on the Purchasing and Sale Power

Constraints are constructed in this part to ensure the reliability of the connection between the microgrid and the external grid.

$$0 \le P_{\mathrm{M},t}^{\mathrm{buy}} \le \chi_{\mathrm{M},t} \cdot P_{\mathrm{M}}^{\mathrm{buy,max}} \tag{22}$$

$$0 \le P_{\mathrm{M},t}^{\mathrm{sell}} \le (1-\chi_{\mathrm{M},t}) \cdot P_{\mathrm{M}}^{\mathrm{sell,max}} \tag{23}$$

where $P_{\mathrm{M}}^{\mathrm{buy,max}}$ and $P_{\mathrm{M}}^{\mathrm{sell,max}}$ represent the upper limits of purchasing and selling power of the microgrid, respectively. $\chi_{\mathrm{M},t}$ is a binary variable, whose value is 1 indicating that the microgrid buys power from the distribution network.

2.3. Objective Function of the Microgrid Planning

The objective function of the microgrid-planning model is shown in Equation (24), which is divided into two stages to be solved. The objective function of the first stage is the lowest cost of initial investment cost, and the second stage is the lowest cost of the dispatching operation.

$$\min_{n}\left(C^{\mathrm{inv}} + \max_{u} \min_{x,y,z} C_{\mathrm{open}}\right) \tag{24}$$

where C^{inv} is the total initial investment cost of the microgrid. C_{open} denotes the operation and maintenance costs of the microgrid. $\boldsymbol{x}$, $\boldsymbol{y}$, $\boldsymbol{z}$ and $\boldsymbol{n}$ are the sets of optimized variables, and $\boldsymbol{u}$ is the set of uncertainties; particularly, $\boldsymbol{n} = \left[E_{\mathrm{bat}}^{\mathrm{max}}, P_{\mathrm{wt}}^{\mathrm{max}}, P_{\mathrm{pv}}^{\mathrm{max}}, P_{\mathrm{load}}^{\mathrm{max}}\right]^{\mathrm{T}}$, $\boldsymbol{u} = \left[P_{\mathrm{wt},t}, P_{\mathrm{pv},t}, P_{\mathrm{load},t}\right]^{\mathrm{T}}$, $\boldsymbol{x} = \left[P_{\mathrm{bat},t}^{\mathrm{dis}}, P_{\mathrm{bat},t}^{\mathrm{ch}}, P_{\mathrm{M},t}^{\mathrm{buy}}, P_{\mathrm{M},t}^{\mathrm{sell}}, P_{\mathrm{G},t}, \mathrm{SOC}_t\right]^{\mathrm{T}}$, $\boldsymbol{y} = \left[\chi_{\mathrm{bat},t}, \chi_{\mathrm{M},t}, \chi_{\mathrm{SOC},t}^{1}, \cdots, \chi_{\mathrm{SOC},t}^{d}, \cdots, \chi_{\mathrm{SOC},t}^{D}\right]^{\mathrm{T}}$ and $\boldsymbol{z} = \left[DOD_t^1, \cdots, DOD_t^d, \cdots, DOD_t^D\right]^{\mathrm{T}}$.

2.3.1. Initial Investment Cost

The initial investment cost includes the installation costs of WT, PV, ESS and MT, as shown in Equations (25)–(28).

$$C^{\mathrm{inv}} = C_{\mathrm{bat}}^{\mathrm{inv}} + C_{\mathrm{en}}^{\mathrm{inv}} \tag{25}$$

$$C_{\mathrm{en}}^{\mathrm{inv}} = P_{\mathrm{G}}^{\mathrm{max}} c_{\mathrm{G}} F_{\mathrm{CRE}}(r_{\mathrm{G}}, Y_{\mathrm{G}}) + P_{\mathrm{pv}}^{\mathrm{max}} c_{\mathrm{pv}} F_{\mathrm{CRE}}(r_{\mathrm{pv}}, Y_{\mathrm{pv}}) + P_{\mathrm{wt}}^{\mathrm{max}} c_{\mathrm{wt}} F_{\mathrm{CRE}}(r_{\mathrm{wt}}, Y_{\mathrm{wt}}) \tag{26}$$

$$C_{\mathrm{bat}}^{\mathrm{inv}} = E_{\mathrm{bat}}^{\mathrm{max}} c_{\mathrm{bat}} F_{\mathrm{CRE}}(r_{\mathrm{bat}}, Y_{\mathrm{bat}}) \tag{27}$$

$$F(r, Y) = \frac{r(1+r)^Y}{(1+r)^Y - 1} \tag{28}$$

where $C_{\mathrm{bat}}^{\mathrm{inv}}$ and $C_{\mathrm{en}}^{\mathrm{inv}}$ are investment costs of the ESS and power sources, respectively. $E_{\mathrm{bat}}^{\mathrm{max}}$ is the maximum capacity of the ESS. $F_{\mathrm{CRE}}(r, Y)$ is the net present value of the annual investment [32]. r and Y are the discount rate and the number of discounted years of equipment, respectively, among which the number of discounted years of the ESS is the floating charge life [33]. In the lifetime model of the energy storage system, particularly for the battery, the value of the floating charge life is set to 10 [29,33].

2.3.2. Equipment Operation and Maintenance Costs

The total equipment operation and maintenance cost C_{open} includes the operating costs of the MT $C_{\mathrm{G}}^{\mathrm{open}}$, the costs of purchasing and selling power of the microgrid C_{grid}, the costs of equipment maintenance C_{op}, as well as the cost of environmental governance C_{po}, respectively.

$$C_{\mathrm{open}} = C_{\mathrm{G}}^{\mathrm{open}} + C_{\mathrm{grid}} + C_{\mathrm{op}} + C_{\mathrm{po}} \tag{29}$$

$$C_{\mathrm{G}}^{\mathrm{open}} = \sum_{t=1}^{T} c_{\mathrm{fuel},t} \cdot P_{\mathrm{G},t} \tag{30}$$

$$C_{\text{grid}} = \sum_{t=1}^{T} \left(c_{\text{buy},t} P_{\text{M},t}^{\text{buy}} \Delta t - c_{\text{sell},t} P_{\text{M},t}^{\text{sell}} \Delta t \right) \tag{31}$$

$$C_{\text{op}} = \sum_{i=1}^{4} c_{\text{op}}^{i} \cdot P_{i,t} \tag{32}$$

$$C_{\text{po}} = \sum_{t=1}^{T} \sum_{n=1}^{N} k_{n,t} \cdot c_{n,t} \cdot P_{\text{G},t} \tag{33}$$

where $\mathrm{c}_{\text{fuel},t}$ is the cost of fuel during period t. $k_{n,t}$ and $c_{n,t}$ are the discharging amount of the nth pollutant and its unit price of pollution abatement of the MT during period t, respectively. $C_{\text{buy},t}$ and $c_{\text{sell},t}$ represent the unit price of power purchase and sale during period t, respectively. C_{op}^{i} and $P_{i,t}$ are the unit prices of maintenance cost and the power of ESS, WT, PV and MT during period t, respectively.

2.4. Solution of Two-Stage Robust Planning

Since the robust planning is a large-scale nonconvex and nonlinear optimization problem, binary variables are introduced in the model to recast it to a mixed integer linear optimization (MILP), as shown in Equations (10) and (11). The MILP model's inner layer, as shown in Equation (24), is a function of the form "max-min"; although the objective function and constraints of the model are linear, the model is non-convex optimization.

In order to solve the above model, the inner layer model is transformed into a single layer model by using the KKT method; then, the model is solved by the C&CG algorithm. Compared with Benders decomposition algorithm, the C&CG algorithm can continuously introduce variables and constraints related to the subproblem when solving the master problem, thus obtaining a more compact lower bound of the originally objective function and effectively reducing the number of iterations.

Considering the above constraints, the simplified form of the original problem is shown in Equation (34). Particularly, the worst-case scenario is the one in which the value of u is taken such that the objective function maximizes.

$$\begin{gathered} \min_{n} \left(C^{\text{inv}} + \max_{u} \min_{x,y,z} \boldsymbol{C}^{\mathrm{T}} \boldsymbol{x} \right) \\ s.t. \begin{cases} \boldsymbol{Ax} \le \boldsymbol{a} \\ \boldsymbol{Bx} = 0 \\ \boldsymbol{E}_1 \boldsymbol{x} + \boldsymbol{E}_2 \boldsymbol{y} \le \boldsymbol{e} \\ \boldsymbol{F}_1 \boldsymbol{x} + \boldsymbol{F}_2 \boldsymbol{u} = 0 \\ \boldsymbol{H}_1 \boldsymbol{z} + \boldsymbol{H}_2 \boldsymbol{y} \le \boldsymbol{h} \\ \boldsymbol{In} \le \boldsymbol{i} \\ \boldsymbol{n},\boldsymbol{u},\boldsymbol{x},\boldsymbol{z} \ge 0, \boldsymbol{y} \in \{0,1\} \end{cases} \end{gathered} \tag{34}$$

where $\boldsymbol{A}$, $\boldsymbol{B}$, $\boldsymbol{E}_1$, $\boldsymbol{E}_2$, $\boldsymbol{F}_1$, $\boldsymbol{F}_2$, $\boldsymbol{H}_1$, $\boldsymbol{H}_2$, $\boldsymbol{a}$, $\boldsymbol{e}$ and $\boldsymbol{h}$ are the constant matrices.

The two-layer CC&G algorithm is used to solve the model, and the inner loop is used to find the most serious scenario and return it to the main problem, namely the subproblem; the outer cycle is used to solve the planning scheme containing all the obtained scenarios, namely the master problem.

2.4.1. Solution of the Master Problem

Every time a subproblem in the model finds the worst scenario, new variables are introduced in the master problem, and then the master problem can be solved. The simplified form of the master problem is as follows:

$$\begin{aligned}
&\min_{n}\left(C^{\mathrm{inv}}+\alpha\right)\\
&s.t.\begin{cases}
\alpha \geq \boldsymbol{C}^{T}\boldsymbol{x}_{l}\\
\boldsymbol{A}\boldsymbol{x}_{l}\leq \boldsymbol{a}\\
\boldsymbol{B}\boldsymbol{x}_{l}=0\\
\boldsymbol{E}_{1}\boldsymbol{x}_{l}+\boldsymbol{E}_{2}\boldsymbol{y}\leq \boldsymbol{e}\\
\boldsymbol{F}_{1}\boldsymbol{x}_{l}+\boldsymbol{F}_{2}\boldsymbol{u}_{l}=0\\
\boldsymbol{H}_{1}\boldsymbol{z}_{l}+\boldsymbol{H}_{2}\boldsymbol{y}_{l}\leq \boldsymbol{h}\\
\boldsymbol{I}\boldsymbol{n}\leq \boldsymbol{i}\\
\boldsymbol{n},\boldsymbol{u}_{l},\boldsymbol{x}_{l},\boldsymbol{z}_{l}\geq 0,\boldsymbol{y}\in\{0,1\},\forall l\leq l_{\max}
\end{cases}
\end{aligned} \tag{35}$$

where α is the auxiliary variable of the subproblem. l and $l_{\max}$ are the real-time value and maximum value of the iterations, respectively. $\boldsymbol{n}_l$, $\boldsymbol{u}_l$, $\boldsymbol{x}_l$ and $\boldsymbol{z}_l$ are the solutions of the subproblem after the lth iteration. $\boldsymbol{u}_l$ is the worst scenario found in the uncertainty set.

The master problem solves the upper bound of the objective function, while the subproblem solves the lower bound, which are UB_{mas} and LB_{mas}, respectively. If the boundary of the objective function satisfies Equation (36), then the iterative calculation of the master problem is terminated.

$$|UB_{\mathrm{mas}}-LB_{\mathrm{mas}}|\leq \xi \tag{36}$$

2.4.2. Solution of the Subproblem

The subproblem is used to find the worst scenario and return it to the master problem, as shown in Equation (37).

$$\begin{aligned}
&\max_{u}\min_{x,y,z}\boldsymbol{C}^{T}\boldsymbol{x}\\
&s.t.\begin{cases}
\boldsymbol{A}\boldsymbol{x}\leq \boldsymbol{a}\\
\boldsymbol{B}\boldsymbol{x}=0\\
\boldsymbol{E}_{1}\boldsymbol{x}+\boldsymbol{E}_{2}\boldsymbol{y}\leq \boldsymbol{e}\\
\boldsymbol{F}_{1}\boldsymbol{x}+\boldsymbol{F}_{2}\boldsymbol{u}=0\\
\boldsymbol{H}_{1}\boldsymbol{z}+\boldsymbol{H}_{2}\boldsymbol{y}\leq \boldsymbol{h}\\
\boldsymbol{u},\boldsymbol{x},\boldsymbol{z}\geq 0,\boldsymbol{y}\in\{0,1\}
\end{cases}
\end{aligned} \tag{37}$$

The inner layer of the subproblem contains binary variables $\boldsymbol{y}$, which cannot be directly converted into a single-layer model by the KKT method [34]. The solution steps are shown as follows:

(1) Linearization of the subproblem

In Equation (37), the binary variable is set to an initial value, and the upper and lower value of the subproblem are set to $UB_{\mathrm{sub}}=+\infty$ and $LB_{\mathrm{sub}}=-\infty$, respectively, and then, the subproblem becomes a linear optimization problem and can be transformed by KKT method.

(2) Solve the outer layer of the subproblem

The subproblem of Equation (37) can be transformed in Equation (38), which is used to update the upper bound value $UB_{\text{sub}}= \tau$.

$$\max_{u,x,z} \tau$$
$$s.t.\begin{cases} \tau \leq \boldsymbol{C}^{T}\boldsymbol{x} \\ \boldsymbol{A}\boldsymbol{x}_k \leq \boldsymbol{a} \\ \boldsymbol{B}\boldsymbol{x}_k = 0 \\ \boldsymbol{E}_1\boldsymbol{x}_k + \boldsymbol{E}_2\boldsymbol{y}_{k^*} \leq \boldsymbol{e} \\ \boldsymbol{F}_1\boldsymbol{x}_k + \boldsymbol{F}_2\boldsymbol{u}_k = 0 \\ \boldsymbol{H}_1\boldsymbol{z}_k + \boldsymbol{H}_2\boldsymbol{y}_{k^*} \leq \boldsymbol{h} \\ \boldsymbol{u}_k, \boldsymbol{x}_k, \boldsymbol{z}_k \geq 0, 1 \leq k \end{cases} \tag{38}$$

where τ is the optimal solution of the subproblem in the objective function. k is the iteration number of the subproblem's inner loop. $\boldsymbol{y}_{k^*}$ is the initial value of $\boldsymbol{y}$.

The dual multiplier is introduced in Equation (38), the following constraints are added:

$$s.t.\begin{cases} \boldsymbol{E}_2^{\mathrm{T}}\cdot\lambda_1 = \boldsymbol{C}^{\mathrm{T}} \\ (\boldsymbol{E}_1 x_k + \boldsymbol{E}_2\boldsymbol{y}_{k^*} - \boldsymbol{e})\cdot\lambda_{1,k} = 0 \\ \boldsymbol{H}_2^{\mathrm{T}}\cdot\lambda_2 = \boldsymbol{C}^{\mathrm{T}} \\ (\boldsymbol{H}_1 z_k + \boldsymbol{H}_2\boldsymbol{y}_{k^*} - \boldsymbol{h})\cdot\lambda_{2,k} = 0 \end{cases} \tag{39}$$

where $\boldsymbol{\lambda}_{1,k}$ and $\boldsymbol{\lambda}_{2,k}$ are the dual variables of the kth iteration respectively. In particular, if the values of $(\boldsymbol{E}_1\boldsymbol{x}_k+\boldsymbol{E}_2\boldsymbol{y}_{k^*}- \boldsymbol{e})$ and $(\boldsymbol{H}_1\boldsymbol{z}_k+\boldsymbol{H}_2\boldsymbol{y}_{k^*}-\boldsymbol{h})$ are 0, then $\boldsymbol{\lambda}_{1,k}$ and $\boldsymbol{\lambda}_{2,k}$ are unconstrained, respectively. If the values of $(\boldsymbol{E}_1\boldsymbol{x}_k+\boldsymbol{E}_2\boldsymbol{y}_{k^*}-\boldsymbol{e})$ and $(\boldsymbol{H}_1\boldsymbol{z}_k+\boldsymbol{H}_2\boldsymbol{y}_{k^*}-\boldsymbol{h})$ are not 0, then the values of $\boldsymbol{\lambda}_{1,k}$ and $\boldsymbol{\lambda}_{2,k}$ are 0, respectively.

Then they can be linearized by the Big M method, as shown in Equation (40).

$$s.t.\begin{cases} \lambda_{1,k} \leq M(1-\sigma) \\ \boldsymbol{E}_1\boldsymbol{x}_k + \boldsymbol{E}_2\boldsymbol{y}_{k^*} - \boldsymbol{e} \leq M\sigma \\ \lambda_{2,k} \leq M(1-\sigma) \\ \boldsymbol{H}_1\boldsymbol{z}_k + \boldsymbol{H}_2\boldsymbol{y}_{k^*} - \boldsymbol{h} \leq M\sigma \end{cases} \tag{40}$$

where M is a big positive number. σ is a binary variable.

(3) Solve the inner layer of the subproblem

The scenario is substituted into the inner layer of the subproblem, as shown in Equation (41); and the equation is solved to update $LB_{\text{sub}}= \max\left\{LB_{\text{sub}},\ \boldsymbol{C}^{\mathrm{T}}x\right\}$.

$$\min_{x,y,z} \boldsymbol{C}^{T}\boldsymbol{x}$$
$$s.t.\begin{cases} \boldsymbol{A}\boldsymbol{x} \leq \boldsymbol{a} \\ \boldsymbol{B}\boldsymbol{x} = 0 \\ \boldsymbol{E}_1\boldsymbol{x} + \boldsymbol{E}_2\boldsymbol{y} \leq \boldsymbol{e} \\ \boldsymbol{F}_1\boldsymbol{x} + \boldsymbol{F}_2\hat{\boldsymbol{u}} = 0 \\ \boldsymbol{H}_1\boldsymbol{z} + \boldsymbol{H}_2\boldsymbol{y} \leq \boldsymbol{h} \\ \hat{\boldsymbol{u}}, \boldsymbol{x}, \boldsymbol{z} \geq 0, \boldsymbol{y} \in \{0,1\} \end{cases} \tag{41}$$

where $\hat{\boldsymbol{u}}$ is the scenario calculated by Equation (38).

(4) Criteria for the subproblem's iteration

If UB_{sub} and LB_{sub} satisfy Equation (42), the iteration is terminated and UB_{sub} is returned to the main problem, that is, $UB_{\text{sub}}= UB_{\text{mas}}$; otherwise, $\boldsymbol{x}_k$, z_k and $\boldsymbol{u}_k$ are recreated respectively, $k = k + 1$, and the subproblem's iteration is restarted.

$$|UB_{\text{sub}} - LB_{\text{sub}}| \leq \xi \tag{42}$$

2.4.3. Solving Process of the Robust Model

Based on the above analysis, the algorithm flow of the proposed model is shown as follows:

(1) Convert the objective function to a MILP problem; as for the master problem, set l = 0, $UB_{\text{mas}} = +\infty$ and $LB_{\text{mas}} = -\infty$; as for the subproblem, k = 0, $UB_{\text{sub}} = +\infty$ and $LB_{\text{sub}} = -\infty$.

(2) Solve the master problem and update $LB_{\text{mas}} = C^{\text{inv}} + \alpha$.

(3) Set the initial value of the binary variable and solve the outer layer of the subproblem, that is, solve the Equation (38). If the equation is successfully solved, $UB_{\text{sub}} = \tau$ and return $\hat{\boldsymbol{u}}$ to (4); otherwise, return $\hat{\boldsymbol{u}}$ to the Equation (35), and return to (2).

(4) Solve the inner layer of the subproblem, that is, solve the Equation (41); and update $LB_{\text{sub}} = \max\left\{LB_{\text{sub}}, \boldsymbol{C}^{\text{T}}x\right\}$.

(5) If $|\text{UB}_{\text{sub}} - \text{LB}_{\text{sub}}| \leq \xi$, $\text{UB}_{\text{sub}} = \text{UB}_{\text{mas}}$ and go to (6); otherwise, $k = k + 1$ and return to (3).

(6) If $|\text{UB}_{\text{mas}} - \text{LB}_{\text{mas}}| \leq \xi$, output the optimal planning scheme; otherwise, return $\hat{\boldsymbol{u}}$ to (2) and $l = l + 1$.

The flow chart of the proposed model is shown in Figure 2.

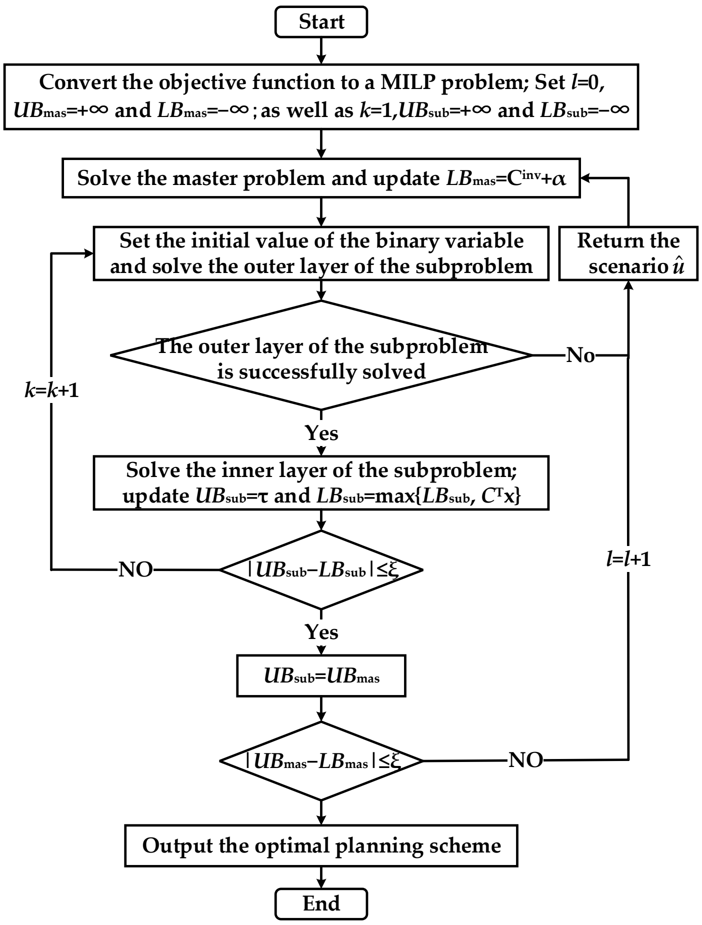

Figure 2. The flow chart of the two-stage robust model.

3. Construction of IGRA Based on the Robust Microgrid-Planning Model

GRA is used to judge whether the connection between different series is close according to the similarity degrees of the geometric curves. This theory can effectively overcome the shortcomings of mathematical statistics methods, such as requiring large amounts of data, samples to obey a probability distribution and a large amount of calculation.

According to GRA, if a system contains data with dynamically random variation characteristics, the system can be called a grey system. The relational degrees between the indicators in the grey system can be obtained by relational analysis; particularly, the relational degrees can indirectly map the change characteristics of the grey system. In this paper, renewable energy with randomly variable characteristics can be regarded as grey data, and the system in which renewable energy resides can be regarded as a grey system; then, the relational degrees are used as the reference indices of the boundary setting of uncertainty sets, and can indirectly map the change characteristics of the microgrid planning.

3.1. Grey Relational Analysis with the Microgrid-Planning Model

This part focuses on using traditional GPA to analyze the relational degrees of microgrid planning. It should be noted that this paper simulates multi-scenario microgrid planning by changing the robustness parameters, and carries out relational degrees for each individual cost and total cost. The main calculation steps are as follows.

(1) Generation of the analysis matrix

The index sequence $\boldsymbol{C}_{\text{to}}= [C_{\text{to}}(1),\ C_{\text{to}}(2),\ \cdots,\ C_{\text{to}}(n)]^{\text{T}}$ is composed of the total planning costs under n scenarios; the index sequence $\boldsymbol{C}_{\text{si}}= \left[\boldsymbol{C}_{\text{si},1},\ \boldsymbol{C}_{\text{si},2},\ \cdots,\ \boldsymbol{C}_{\text{si},b}\right]$ consists of b single planning costs under n scenarios, especially $\boldsymbol{C}_{\text{si},b}= [C_{\text{si},b}(1),\ C_{\text{si},b}(2),\ \cdots,\ C_{\text{si},b}(n)]^{\text{T}}$. The analysis matrix $\boldsymbol{C}_{\text{an}}$ is shown in Equation (43).

$$\boldsymbol{C}_{\text{an}} = (\boldsymbol{C}_{\text{to}},\ \boldsymbol{C}_{\text{si},1},\ \cdots,\ \boldsymbol{C}_{\text{si},b})_{n*(b+1)} \quad (43)$$

(2) Generation of the initial value matrix

Before the relational analysis, the data of the analysis matrix need to be normalized. The above data is adopted by initialization in this paper, and the initial value matrix $\boldsymbol{C}_{\text{in}}$ is shown in Equation (44), especially $\boldsymbol{C}'_{\text{to}}= [C'_{\text{to}}(1),\ C'_{\text{to}}(2),\ \cdots,\ C'_{\text{to}}(n)]^{\text{T}}$ and $\boldsymbol{C}'_{\text{si},b}= \left[\boldsymbol{C}'_{\text{si},b}(1),\ \boldsymbol{C}'_{\text{si},b}(2),\ \cdots,\ \boldsymbol{C}'_{\text{si},b}(n)\right]^{\text{T}}$.

$$\boldsymbol{C}_{\text{in}} = \left(\boldsymbol{C}'_{\text{to}},\ \boldsymbol{C}'_{\text{si},1},\ \cdots,\ \boldsymbol{C}'_{\text{si},b}\right)_{n*(b+1)} \quad (44)$$

(3) Generation of the difference matrix

The difference matrix $\boldsymbol{C}_{\text{di}}$ is shown in Equation (45), especially $\boldsymbol{C}_{\text{di},b} = [C_{\text{di},b}(1),\ C_{\text{di},b}(2),\ \cdots,\ C_{\text{di},b}(\text{n})]^{\text{T}}$. The difference operation is carried out on the data in the initial value matrix, according to Equation (46), that is, the absolute differences between the total costs and each individual cost are calculated, respectively.

$$\boldsymbol{C}_{\text{di}} = [\boldsymbol{C}_{\text{di},1},\ \boldsymbol{C}_{\text{di},2},\ \cdots,\ \boldsymbol{C}_{\text{di},b}]_{n*b} \quad (45)$$

$$C_{\text{di},b}(n) = \left|C'_{\text{to}}(n) - C'_{\text{si},b}(n)\right| \quad (46)$$

The maximum value $C_{\text{di}}^{\max}$ and minimum value $C_{\text{di}}^{\min}$ of the difference matrix C_{di} are calculated by the following:

$$C_{\text{di}}^{\max} = \max\mathbf{C}_{\text{di}} \quad (47)$$

$$C_{\text{di}}^{\min} = \min\mathbf{C}_{\text{di}} \quad (48)$$

(4) Calculation of the grey relational coefficient

The relational coefficient $\lambda_b(n)$ between the single planning cost bth and the total cost is calculated by Equation (49) in scenario nth. Then, all calculated results obtained by using Equation (49) form the relational coefficient matrix $\boldsymbol{C}_{\mathrm{re}}$, as shown in, especially, $\boldsymbol{C}_{\mathrm{re},b}= [C_{\mathrm{re},b}(1),\ C_{\mathrm{re},b}(2),\ \cdots,\ C_{\mathrm{re},b}(n)]^{\mathrm{T}}$.

$$C_{\mathrm{re},b}(n) = \frac{C_{\mathrm{di}}^{\min} + \rho C_{\mathrm{di}}^{\max}}{C_{\mathrm{di},b}(n) + \rho C_{\mathrm{di}}^{\max}} \tag{49}$$

$$\boldsymbol{C}_{\mathrm{re}} = [\boldsymbol{C}_{\mathrm{re},1},\ \boldsymbol{C}_{\mathrm{re},1},\ \cdots,\ \boldsymbol{C}_{\mathrm{re},1}]_{n*b} \tag{50}$$

where ρ is known as the identification coefficient, whose value is from 0 to 1, and its value is 0.5 in the traditional GPA.

By taking the mean value of each column in the relational coefficient matrix $\boldsymbol{C}_{\mathrm{re}}$, as shown in Equation (51), the grey relational degrees between each individual cost and the total cost are obtained.

$$R_b = \frac{1}{n}\sum_{i=1}^{n} C_{\mathrm{re},b}(i) \tag{51}$$

3.2. Entropy Weight Method with the Microgrid-Planning Model

The EWM can make use of the information reflected by the objective data to assign weights; particularly, the higher the dispersion degree of data, the greater the weight of this index. Compared with AHP, EWM has higher accuracy and adaptability, and has effective guidance for the microgrid-planning modification.

As for the same change of the robustness parameters, the more discrete the planning cost, the greater the effect on the total cost, which indirectly reflects the effects of the above uncertainties with the same robustness on the microgrid-planning costs. Therefore, when the weight of all indicators is redistributed, the higher weights should be assigned to the above costs, and combined into the GRA to obtain the relational degree of different uncertainties with the same robustness parameter to the total cost.

3.2.1. Generation of the Initial Matrix and Normalization of Its Data

Firstly, the index sequence $\boldsymbol{C}_{\mathrm{si}}= \left[\boldsymbol{C}_{\mathrm{si},1},\ \boldsymbol{C}_{\mathrm{si},2},\ \cdots,\ \boldsymbol{C}_{\mathrm{si},b}\right]$ mentioned above is taken as the initial matrix of the EWM. Then, the data inside the initial matrix is normalized by using the range method, in which Equation (52) is used for negative indicators and Equation (53) is used for positive indicators. The dimensionless matrix is $\boldsymbol{C}_{\mathrm{no}}= \left[\boldsymbol{C}_{\mathrm{no},1},\ \boldsymbol{C}_{\mathrm{no},2}, \ldots,\ \boldsymbol{C}_{\mathrm{no},b}\right]$, especially $\boldsymbol{C}_{\mathrm{no},b}= \left[\hat{C}_{\mathrm{si},b}(1),\ \hat{C}_{\mathrm{si},b}(2),\ \cdots,\ \hat{C}_{\mathrm{si},b}(n)\right]^{\mathrm{T}}$.

$$\hat{C}_{\mathrm{si},b}(n) = \frac{C_{\mathrm{si},b}^{\max} - C_{\mathrm{si},b}(n)}{C_{\mathrm{si},b}^{\max} - C_{\mathrm{si},b}^{\min}} \tag{52}$$

$$\hat{C}_{\mathrm{si},b}(n) = \frac{C_{\mathrm{si},b}(n) - C_{\mathrm{si},b}^{\min}}{C_{\mathrm{si},b}^{\max} - C_{\mathrm{si},b}^{\min}} \tag{53}$$

where $C_{\mathrm{si},b}^{\max}$ and $C_{\mathrm{si},b}^{\min}$ are the maximum and minimum values of the column where $C_{\mathrm{si},b}$ resides, respectively.

Finally, the proportion of each planning cost in the total cost is calculated according to Equation (54). The proportionality matrix is $\boldsymbol{C}_{\mathrm{pr}}= \left[\boldsymbol{C}_{\mathrm{pr},1},\ \boldsymbol{C}_{\mathrm{pr},2},\ \ldots,\ \boldsymbol{C}_{\mathrm{pr},b}\right]$, especially $\boldsymbol{C}_{\mathrm{pr},b}= [C_{\mathrm{pr},b}(1),\ C_{\mathrm{pr},b}(2),\ \ldots,\ C_{\mathrm{pr},b}(n)]^{\mathrm{T}}$.

$$C_{\mathrm{pr},b}(n) = \frac{\hat{C}_{\mathrm{si},b}(n)}{\sum_{i=1}^{n} \hat{C}_{\mathrm{si},b}(i)} \tag{54}$$

3.2.2. Calculation of Information Entropy and Weighting Coefficient

The information entropy $C_{\mathrm{en,b}}$ of the bth planning cost is calculated according to Equation (55), and the matrix of all information entropy is $\boldsymbol{C}_{\mathrm{en}} = \left[C_{\mathrm{en},1},\ C_{\mathrm{en},2},\ \ldots,\ C_{\mathrm{en},b}\right]^{\mathrm{T}}$; particularly, $k = 1/\ln n$ can make the information entropy between [0, 1] when the data of indicators are identical.

$$C_{\mathrm{en},b} = k\sum\nolimits_{i=1}^{n} C_{\mathrm{pr},b}(i)\cdot \ln C_{\mathrm{pr},b}(i) \tag{55}$$

Finally, the entropy weight of the bth planning cost is calculated according to Equation (56).

$$C_{\mathrm{ew},b} = \frac{1 - C_{\mathrm{en},b}}{\sum_{i=1}^{b}\left(1 - C_{\mathrm{en},i}\right)} \tag{56}$$

3.3. Improvement of the GRA

The IGRA based on EWM and TF is proposed in this section, in order to improve the accuracy of the grey degrees. In the first part, the identification coefficient of dynamic value is set up with TF; in the second part, the calculation of grey relational degrees combined with EWM is detailed.

(1) Dynamic value of identification coefficient based on TF

The core idea of GPA is to calculate the absolute difference between sequences, because the results reflect the degree of spatial similarity between the sequences [35], that is, the smaller the absolute difference, the greater the relational degree. The relational degree is calculated by a true fraction, as shown in Equation (49); particularly, if the value of ρ is 0.5, the characteristics of the index will be averaged and the accuracy of the model will be reduced; at the same time, the value of the true fraction increases when the number contained in both the numerator and the denominator increases. According to the above theories, for a set of indicators, the absolute difference is negatively correlated with the relational degree.

The trigonometric fuzzy number is used as the referenced function to make the algebraic operation easier, and its membership function is shown as Equation (57). Therefore, based on the membership characteristic of TF theory, a method for dynamic calculation of the identification coefficient is proposed.

$$\mu(T_x) = \begin{cases} (T_x - T_a)/(T_b - T_a) & ,T_a \le T_x \le T_b \\ (T_c - T_x)/(T_c - T_b) & ,T_b \le T_x \le T_c \\ 0 & ,T_x < T_a\ or\ T_b < T_x \end{cases} \tag{57}$$

The triangle fuzzy number is constructed according to the difference value of Equation (46) and the value range of the identification coefficient of Equation (51), as shown in Figure 3.

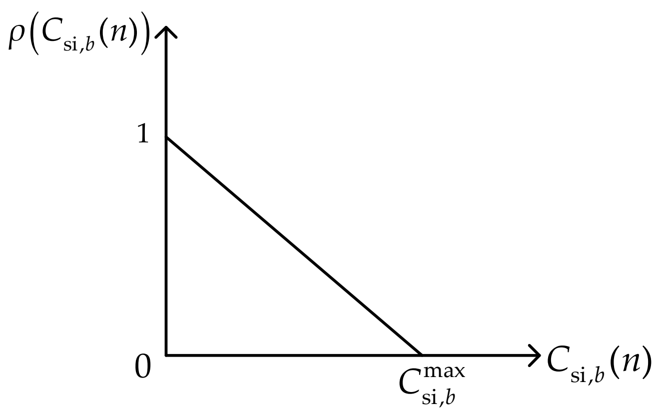

Figure 3. Value of identification coefficient based on triangle fuzzy number.

Since the value of the identification coefficient is in the range (0, 1), the values of the two endpoints are 0.999 and 0.001 here. The value of membership degree $\rho\ (d_b(n))$ is shown in Equation (58).

$$\rho(C_{\mathrm{si},b}(n)) = \begin{cases} 0.999 & ,C_{\mathrm{si},b}(n) = 0 \\ 1 - \frac{C_{\mathrm{si},b}(n)}{C_{\mathrm{si},b}^{\max}} & ,0 < C_{\mathrm{si},b}(n) < C_{\mathrm{si},b}^{\max} \\ 0.001 & ,C_{\mathrm{si},b}(n) = C_{\mathrm{si},b}^{\max} \end{cases} \tag{58}$$

(2) Calculation of grey relational degrees combined with EWM

All the calculation results of Equation (51) and Equation (56) can be expressed as $\boldsymbol{R} = [R_1,\ R_2,\ \ldots,\ R_n]$ and $\boldsymbol{C}_{\mathrm{ew}} = \left[C_{\mathrm{ew},1},\ C_{\mathrm{ew},2},\ \ldots,\ C_{\mathrm{ew},b}\right]$, respectively; then, the final relational degree based on comprehensive weight is calculated according to Equation (59).

$$g_r = [R_1,\ R_2,\ \cdots,\ R_b]\cdot[C_{\mathrm{ew},1},\ C_{\mathrm{ew},2},\ \cdots,\ C_{\mathrm{ew},b}]^T \tag{59}$$

3.4. Solution of the Robust Microgrid-Planning Model's Modification

In this part, the relational degrees between the microgrid-planning costs and robust parameters are introduced in detail. Firstly, the GRA is used to calculate the relational degree between each cost and the total cost of microgrid planning, in the same range of robust parameters. Secondly, the calculation process of EWM is introduced in detail; it is combined with the relational indexes of the previous step, in order to obtain the weight of each cost under the same total cost. Finally, the calculation method of weighted relational degree and the dynamic value method of resolution coefficient are introduced, that is, the construction of IGRA. The calculation procedure is shown as Figure 4.

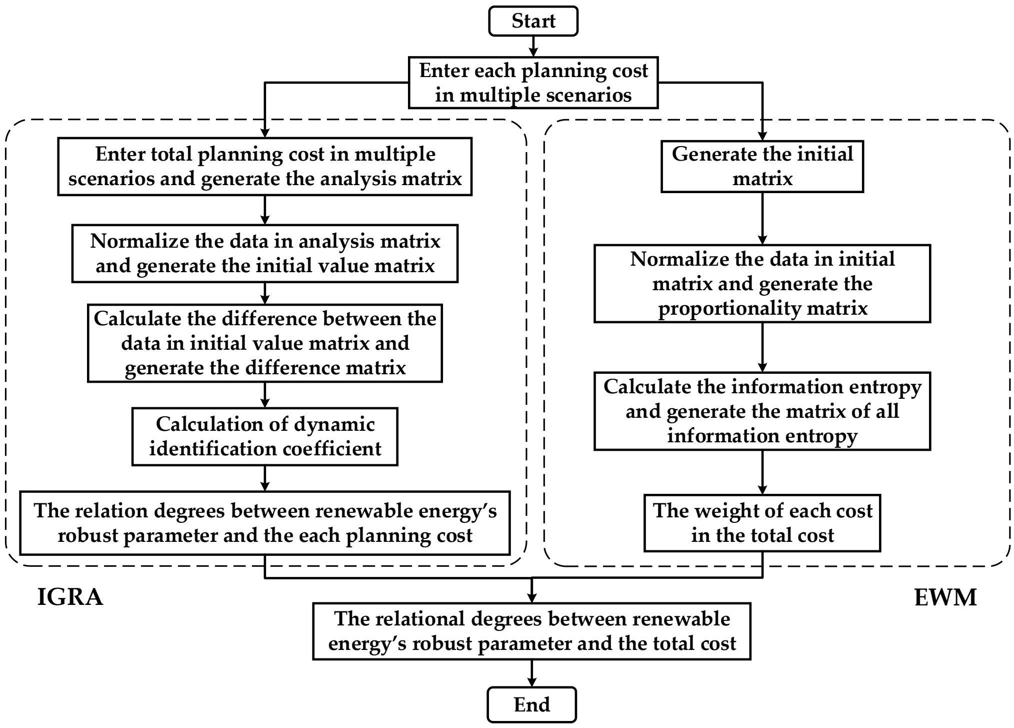

Figure 4. The calculation procedure of relational degrees between renewable energy's robust parameter and the planning cost.

4. Model Solving including the Robust Model and Its Modification Strategy

The two-stage robust planning model's establishment and solution are first detailed. Then, this paper introduces the basis of GRA as a modification method and the method of improvement of its shortcomings; particularly, the calculation process of modification index is detailed by combining the robust planning model's parameters. Based on the above theory, the steps of modifying the robust planning model's robustness parameters are detailed in this section.

(1) The robust planning model with robustness parameters is constructed and solved, according to Figures 1 and 2.

(2) The microgrid-planning schemes under multiple scenarios are simulated by changing the renewable energy's robustness parameters, respectively, and the influences of renewable energy on microgrid planning are analyzed.

(3) The microgrid-planning costs in multiple scenarios are analyzed by IGRA according to Figure 4, namely the construction of reference indices, and the relational degrees between the renewable energy's robustness parameters and each cost component of the microgrid is analyzed.

(4) The robustness parameters are modified by using the relational degrees as a reference for the robustness parameters' weighting, and the planning schemes are compared with the original.

The specific solving steps are shown in Figure 5.

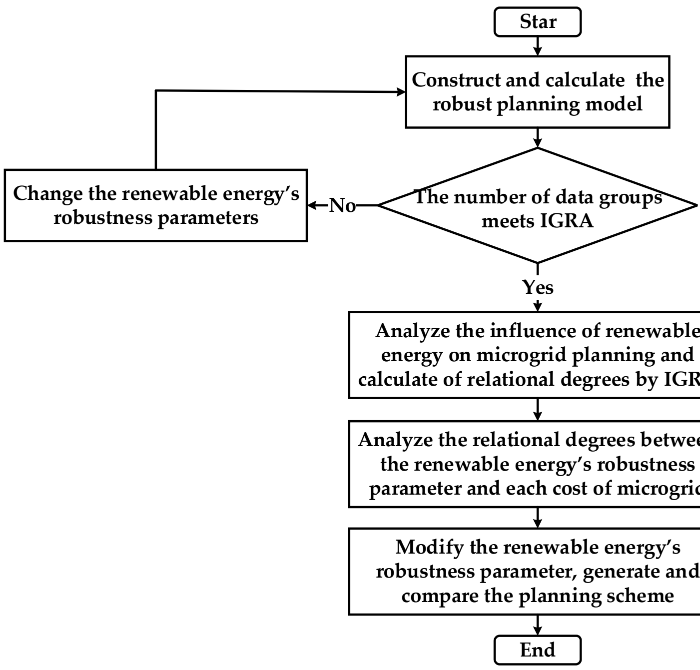

Figure 5. The steps of modifying the robust planning model's robustness parameters.

5. Results and Analysis

Based on the microgrid-planning model built in Figure 1 and the IGRA algorithm, this section verifies the effectiveness of the proposed modification system through the case studies. This section consists of setting parameters of the robust planning mode, verifying the effectiveness of IGRA by comparison, calculating and analyzing the two-stage robust programming model with different renewable energy robustness parameters, modifying the robustness parameters and comparing the planning schemes.

In particular, a real microgrid system in a province of China is taken as a case to calculate, and its parameters are set based on its location and actual operation. The currency of the planning cost is RMB.

5.1. Parameters Description of the Planning Model

In this paper, $\boldsymbol{n} = \left[E_{\text{bat}}^{\max}, P_{\text{wt}}^{\max}, P_{\text{pv}}^{\max}, P_{\text{load}}^{\max}\right]^{\text{T}}$ is the variable to be optimized, that is the proposed microgrid-planning model is a capacity planning model. Based on [36], typical daily values are recommended for the data used in the planning model. Particularly, a typical day is a representative scenario extracted from a large amount of historical resource data of renewables, which reduces the calculation of the planning while retaining valid information [37,38]. The typical daily data is adopted to take place of the annual data in this paper, including: demand-side load and the output of renewable energy, and the data used are all normalized data, as shown in Figure 6.

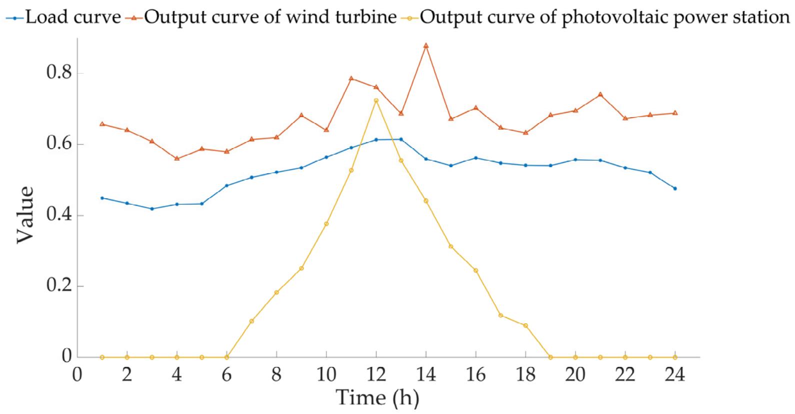

Figure 6. Typical power of the microgrid-planning model.

The typical power price of the microgrid is shown in the Figure 7 [9], which is for the consumption of the demand-side load and microgrid purchasing and sale power.

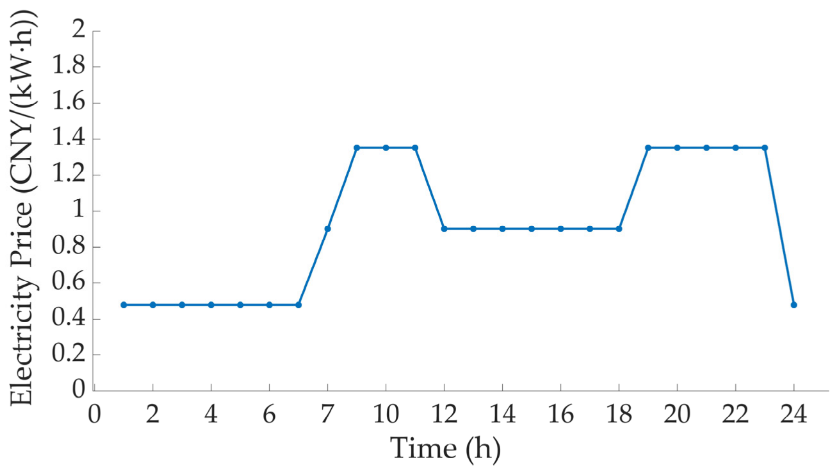

Figure 7. Typical power price of the microgrid-planning model.

The discount rate r of the MT, renewable energy and ESS in this paper is 0.08, and the ratios ε_{ch} and ε_{dis} of the maximum charging and discharging power of the ESS to the maximum capacity are 0.25. The robustness parameter of the demand-side load, Γ_{load}, is always 0.15; and the initial values of the robustness parameters of the WT, Γ_{wt}, and PV, Γ_{pv}, are both 0.05. The planning parameters of each unit are shown in Table 1.

Table 1. Parameters of the planning model.

Element	Name of the Parameter	Numerical Value
MT	P_G^{max}/kW	500
	P_G^{min}/kW	50
	c_{fuel}/(Yuan/(kW·h))	0.6
	Y_G/year	15
Renewable energy	Y_{wt}/year	20
	Y_{pv}/year	15
ESS	SOC^{min}	0.1
	SOC^{max}	0.9
	SOC_{beg} [39]	0.5
	η_{ch}, η_{dis}	0.95
	Y_{bat}/year	10
The power exchanged by the distribution network	$P_M^{sell,max}$/kW	400
	$P_M^{buy,max}$/kW	400

In the planning model, a series of polluting gases is generated during the operation of the MT. The environmental parameters of the microgrid are shown in Table 2.

Table 2. Environmental parameters of the MT.

Polluting Gas	Discharge Coefficient (g/(kW·h))	Governance Cost (Yuan/kg)
CO_2	889	0.210
SO_2	1.8	1.842
NO_x	4.6	62.964

5.2. Improvement Analysis of IGRA

In order to verify the effectiveness and efficiency of the IGRA, this paper uses the data in [40,41]. Firstly, the IGRA and the traditional are used to calculate the relational degrees, as shown in Table 3.

Table 3. Calculation results of relational degree.

Value Method of Identification Coefficient	r_1	r_2	r_3	r_4	r_5
$\rho = 0.5$	0.681	0.664	0.568	0.780	0.731
Dynamic ρ	0.644	0.619	0.424	0.760	0.687

According to the calculation results in Table 3, it can be known that the sequence of relational degrees is: $r_4 > r_5 > r_1 > r_2 > r_3$, which is consistent with the results of [40,41]. The above result proves that the improved algorithm is feasible.

Then, the method and point position in [40] are used to calculate the relational degree between two sequences, as shown in Table 4.

Table 4. Comparison of algorithm results.

	(r_1,r_2)	(r_2,r_3)	(r_1,r_4)	(r_2,r_4)	(r_5,r_4)
$\rho = 0.5$	0.018	0.095	0.099	0.117	0.049
$\rho = 0.458$	0.018	0.096	0.102	0.120	0.051
[40]	0.022	0.083	0.100	0.121	0.064
Dynamic ρ	0.027	0.199	0.117	0.143	0.080

It can be seen from Table 4 that the algorithms proposed in [40,41] have their own advantages and disadvantages. However, the improved algorithm proposed in this paper is superior to the above algorithms.

5.3. Calculation and Analysis of Microgrid Planning Results

Firstly, the initial planning model is generated when $\Gamma_{wt} = \Gamma_{pv} = 0.05$. Secondly, while the robustness parameter of the WT is unchanged ($\Gamma_{wt} = 0.05$), the robustness parameter Γ_{pv} is gradually increased from 0.05 to 0.08, and a series of planning costs affected by the robustness parameter of PV can be obtained. Thirdly, under the same operation as above, a series of planning costs affected by the robustness parameter of WT can be obtained, while Γ_{pv} is 0.05 and Γ_{wt} is gradually increased from 0.05 to 0.08. Finally, the planning costs for all scenarios are shown in Table 5, and the operation plannings are shown in Figures 8–10.

Table 5. Planning results in multiple scenarios.

Γ_{wt}	Γ_{pv}	Cost of the Initial Investment /Yuan	Cost of Equipment Maintenance /Yuan	Cost of Environmental Governance /Yuan	Total Cost /Yuan
0.050	0.050	179,154.07	20,072.35	5300.18	204,526.60
0.050	0.060	179,033.22	20,251.77	5357.24	204,642.23
	0.065	178,696.94	20,867.10	5327.01	204,891.05
	0.070	178,288.53	21,251.08	5373.06	204,912.67
	0.075	178,288.53	21,239.73	5384.40	204,912.66
	0.080	178,272.26	21,369.44	5392.10	205,033.80
0.060	0.050	178,067.16	21,769.91	5402.43	205,239.50
0.065		177,949.69	21,783.52	5434.33	205,167.54
0.070		177,390.89	23,158.29	5461.12	206,010.30
0.075		177,390.89	23,085.89	5533.52	206,010.30
0.080		176,640.39	24,110.56	5485.00	206,235.95

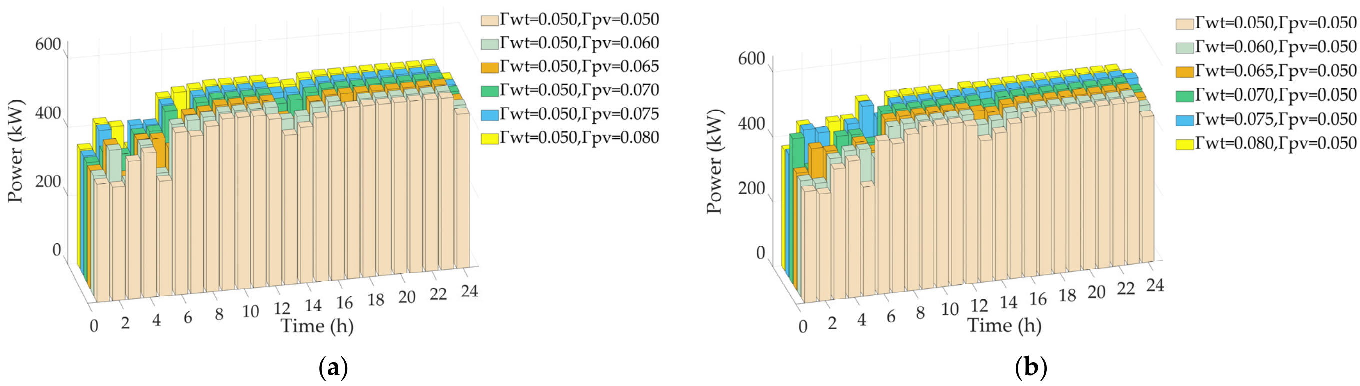

Figure 8. Output planning of the MT in different scenarios. (**a**) Results of microgrid planning for dynamic Γ_{pv}. (**b**) Results of microgrid planning for dynamic Γ_{wt}.

(1) The influence of robustness parameters on planning costs

As can be seen from Table 5, with the increase of robustness-parameter ranges, the total cost of the microgrid planning shows an upward trend, especially the robustness parameter of WT. As for each individual cost, equipment maintenance cost and environmental governance cost also shows a rising trend, while initial investment cost shows a fluctuating trend.

(2) The influence of robustness parameters on operation-planning schemes

As can be seen from Figure 8, with the increase of renewable energy's robustness parameter, the thermal power units all change the output at 0:00–5:00 and 11:00–15:00 to reduce the influence. By comparing (a) and (b) in Figure 8, it can be clearly seen that the robustness parameter of WT has a greater impact on the output planning of thermal power units during the above time period.

As can be seen from Figure 9, in the initial planning model, the microgrid mainly sells power to the distribution network to ensure economic operation and power balance. With the increase of renewable energy's robustness parameter, the power sold at 9:00–11:00 and the night peak hours decreases; especially for WT, as shown in (b) in Figure 9, the microgrid needs to plan to purchase power to maintain power balance during peak hours at night.

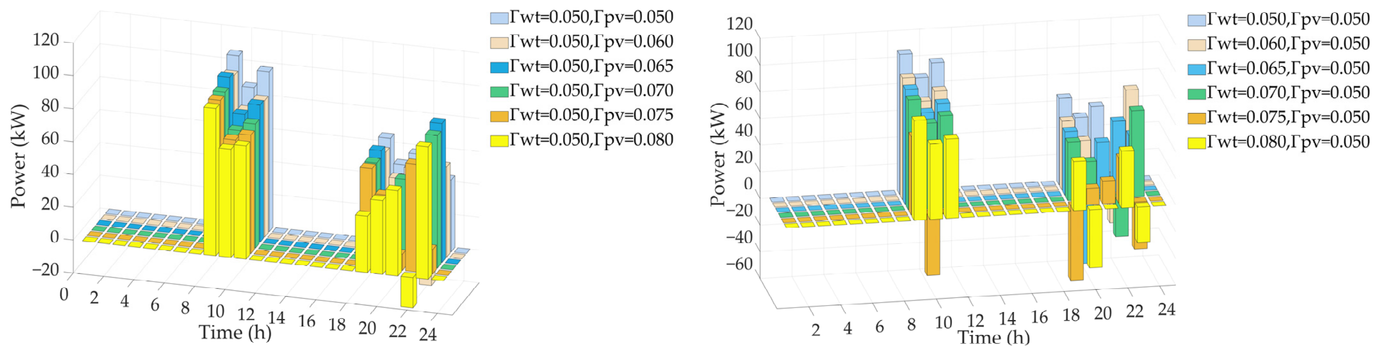

(**a**) (**b**)

Figure 9. Power sold planning by microgrid to distribution network. (**a**) Results of microgrid planning for dynamic Γ_{pv}. (**b**) Results of microgrid planning for dynamic Γ_{wt}.

As can be seen from Figure 10, with the increase of renewable energy's robustness parameter, the switching frequency of charging and discharging state of the ESS increases, which greatly affects the life of the ESS and reflects the intensified instability of the microgrid operation; and the results are especially reflected in the discharging power from 15:00 to 18:00 and the switching frequency of charging-discharging state from 0:00 to 5:00.

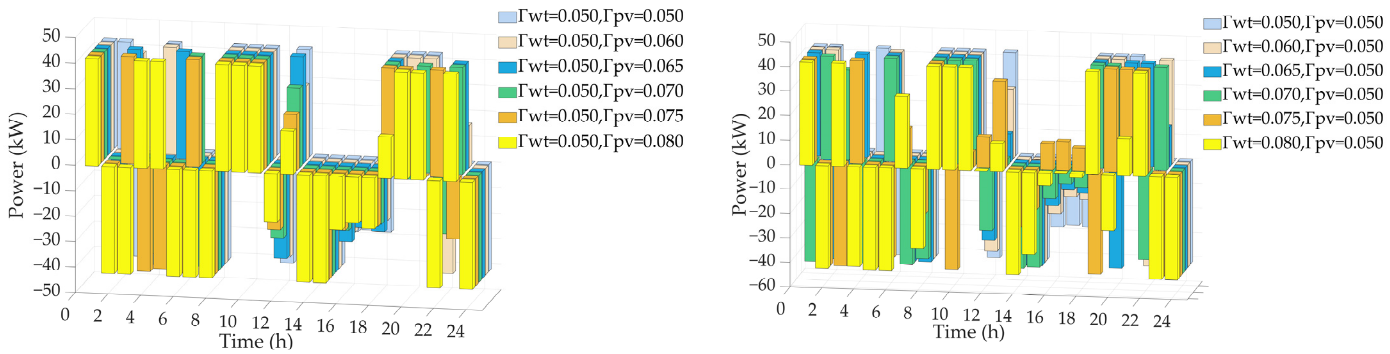

(**a**) (**b**)

Figure 10. Discharging power of ESS by microgrid in different scenarios. (**a**) Results of microgrid planning for dynamic Γ_{pv}. (**b**) Results of microgrid planning for dynamic Γ_{wt}.

The above results show that the types and values of each renewable energy's robustness parameter have different impacts on planning results; that is, the relation between renewable energy's robustness parameters and the change trend of the planning scheme cannot be ignored.

5.4. Calculation and Analysis of Relational Degrees

Based on the data in Table 5, the relational degrees r_{ii}, r_{em} and r_{eg}, which represent the relation between initial investment cost, equipment maintenance cost and environmental treatment cost and total cost, respectively, are calculated by using Equations (43)–(51) and (58). Then, the entropy weight relationship between each cost and total cost is calculated by

Equations (52)–(56). Finally, the weighted total relational degrees r can be obtained according to Equation (59).

(1) Relational analysis between the robustness parameter and each cost.

Through horizontal comparison of the data in Table 6, the orders of relational degree are as follows: $r_{ii,wt} > r_{eg,wt} > r_{em,wt}$ and $r_{ii,pv} > r_{eg,pv} > r_{em,pv}$. The results represent that the fluctuation of each renewable energy has a greater impact on initial investment cost, but little impact on maintenance cost.

Table 6. Relational degrees between robustness parameter and microgrid-planning costs.

Renewable Energy	r_{ii}	r_{em}	r_{eg}	r
PV	0.932	0.413	0.865	0.730
WT	0.951	0.527	0.929	0.798

Through vertical comparison of the data in Table 6, the orders of relational degree are as follows: $r_{ii,wt} > r_{ii,pt}$, $r_{em,wt} > r_{em,pt}$ and $r_{eg,wt} > r_{eg,pt}$. The results represent that the relational degree between the robustness parameter of WT and each economic cost is greater than that of PV.

(2) Relational analysis between the robustness parameter and total cost.

As can be seen from Table 6, the order of relational degree between the robustness parameter of renewable energy and the total cost is as follows: $r_{wt} > r_{pt}$. The relational degree indicates that the comprehensive relation of WT is greater than that of PV.

5.5. Comparative Analysis of the Planning Cost

According to the relational degree obtained, the robustness parameter of the WT has a higher relational degree with microgrid planning, so it is necessary to expand its robustness parameter to improve the ability of WT to adjust the planning cost; the robustness parameter of PV has a lower relational degree with microgrid planning. Based on the data in Table 5, the modified total cost under the corresponding scenario is normalized; the robustness parameter of WT is multiplied by 0.789/0.730, and the robustness parameter of PV is multiplied by 0.730/0.789. The proportions of the revised total cost in the original total cost are shown as Figure 11.

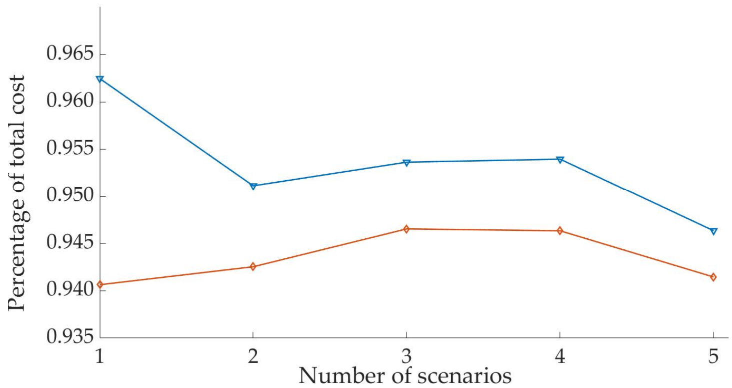

Figure 11. The proportions of the modified total cost in the original total cost.

As can be seen intuitively from Figure 11, the total decline of WT is higher than that of PV; particularly, the average decline of WT and PV are 6.57% and 4.61%, respectively; the modified results are in agreement with the theoretical analysis.

In other ways, when the values of Γ_{pv} are 0.070 and 0.075, respectively, with Γ_{wt} = 0.050, the total costs are very similar; when the values of Γ_{wt} are 0.070 and 0.075, respectively, with Γ_{pv} = 0.050, the total costs are very similar too. As for the modified planning, the declines of the same scenarios are similar. The results show that the magnitude of decline is consistent with the characteristics of renewable energy in the model.

6. Conclusions

In the background of large-scale grid connection of renewable energy, it is necessary to focus on the relation between the differences of renewable energy and microgrid planning. In this paper, a robust microgrid-planning model and its modification strategy based on improved grey relational theory are proposed. The planning model achieves the joint planning of wind-PV-ESS; particularly, the life model of ESS is introduced; and IGRA is constructed with the idea of weight distribution and dynamic values of identification coefficient; the robustness parameters of renewable energy are modified by using the obtained relational degree.

In the analysis section, the dynamic value of identification coefficients can effectively improve the relational degree between indexes; the types and values of renewable energy's robustness parameters have different impacts on planning results. In particular, the relational degree can identify the key renewable energy that influences the costs of grid planning and can modify the renewable energy's robustness parameters to reduce the total cost. In the results section, the total cost is reduced by substituting the modified robustness parameters into the planning model. The subsequent work following this paper will continue to explore the optimal value of the modification coefficients based on GRA.

Author Contributions: Methodology, T.W. and J.X.; software, X.G. and K.L.; validation, G.J.; data curation, Z.X.; writing—original draft preparation, T.W. All authors have read and agreed to the published version of the manuscript.

Funding: This work was supported by the Science and Technology Project of State Grid Anhui Electric Power Co., Ltd. (No. 521209200013).

Institutional Review Board Statement: Not applicable.

Informed Consent Statement: Not applicable.

Data Availability Statement: Data are contained within the article.

Conflicts of Interest: The authors declare no conflict of interest.

Abbreviations

PV	Photovoltaic	ESS	Energy storage system
IGRA	Improved grey relational analysis	RO	Robust optimization
DRO	Distributionally robust optimization	GRA	Grey relational analysis
AHPD	Analytic hierarchy process with Delphi	F-GRA	Fuzzy-Grey Relational Analysis
EWM	Entropy weight method	AHP	Analytic hierarchy process
KKT	Karush–Kuhn–Tucker	C&CG	Column-and-Constraint Generation
WT	Wind turbine	MT	Microturbine
SOC	State of charge	MILP	Mixed integer linear optimization
TF	Triangle fuzzy		

References

1. Olabi, A.G.; Abdelkareem, M.A. Renewable Energy and Climate Change. *Renew. Sustain. Energy Rev.* **2022**, *158*, 112111. [CrossRef]
2. Elavarasan, R.M.; Shafiullah, G.M.; Padmanaban, S.; Kumar, N.M.; Annam, A.; Vetrichelvan, A.M.; Mihet-Popa, L.; Holm-Nielsen, J.B. A Comprehensive Review on Renewable Energy Development, Challenges, and Policies of Leading Indian States with an International Perspective. *IEEE Access* **2020**, *8*, 74432–74457. [CrossRef]
3. Saboori, B.; Gholipour, H.F.; Rasoulinezhad, E.; Ranjbar, O. Renewable Energy Sources and Unemployment Rate: Evidence from the US States. *Energy Policy* **2022**, *168*, 113155. [CrossRef]
4. Kumar, K.; Singh, A. Economic and Experimental Assessment of KCOOH Hybrid Liquid Desiccant-Vapor Compression System. *Sustainability* **2022**, *14*, 15917. [CrossRef]
5. Yanıkoğlu, İ.; Gorissen, B.L.; den Hertog, D. A Survey of Adjustable Robust Optimization. *Eur. J. Oper. Res.* **2019**, *277*, 799–813. [CrossRef]

6. Ding, T.; Liu, S.; Yuan, W.; Bie, Z.; Zeng, B. A Two-Stage Robust Reactive Power Optimization Considering Uncertain Wind Power Integration in Active Distribution Networks. *IEEE Trans. Sustain. Energy* **2015**, *7*, 301–311. [CrossRef]
7. Xiong, P.; Jirutitijaroen, P.; Singh, C. A Distributionally Robust Optimization Model for Unit Commitment Considering Uncertain Wind Power Generation. *IEEE Trans. Power Syst.* **2016**, *32*, 39–49. [CrossRef]
8. Rezaei, N.; Khazali, A.; Mazidi, M.; Ahmadi, A. Economic Energy and Reserve Management of Renewable-Based Microgrids in the Presence of Electric Vehicle Aggregators: A Robust Optimization Approach. *Energy* **2020**, *201*, 117629. [CrossRef]
9. Liu, Y.; Guo, L.; Wang, C. Economic Dispatch of Microgrid Based on Two Stage Robust Optimization. *Proc. CSEE* **2018**, *38*, 4013–4022.
10. Hajebrahimi, A.; Kamwa, I.; Abdelaziz, M.M.A.; Moeini, A. Scenario-Wise Distributionally Robust Optimization for Collaborative Intermittent Resources and Electric Vehicle Aggregator Bidding Strategy. *IEEE Trans. Power Syst.* **2020**, *35*, 3706–3718. [CrossRef]
11. Schreiber, J.; Jessulat, M.; Sick, B. Generative Adversarial Networks for Operational Scenario Planning of Renewable Energy Farms: A Study on Wind and Photovoltaic. In *Proceedings of the International Conference on Artificial Neural Networks*; Springer: Berlin/Heidelberg, Germany, 2019; pp. 550–564.
12. Poolla, B.K.; Hota, A.R.; Bolognani, S.; Callaway, D.S.; Cherukuri, A. Wasserstein Distributionally Robust Look-Ahead Economic Dispatch. *IEEE Trans. Power Syst.* **2020**, *36*, 2010–2022. [CrossRef]
13. Dail, S.; Yec, J.; Fux, H. Distributional Robust Joint Chance Constrained Optimal Capacity Installment of Energy Storage in Power System with High Penetration of Wind Power. *Power Syst. Technol.* **2017**, *41*, 769–777.
14. Wang, R.; Wang, P.; Xiao, G. A Robust Optimization Approach for Energy Generation Scheduling in Microgrids. *Energy Convers. Manag.* **2015**, *106*, 597–607. [CrossRef]
15. Li, S.; Hu, Y. A Multi-Criteria Framework to Evaluate the Sustainability of Renewable Energy: A 2-Tuple Linguistic Grey Relation Model from the Perspective of the Prospect Theory. *Sustainability* **2022**, *14*, 4419. [CrossRef]
16. Sarraf, F.; Nejad, S.H. Improving Performance Evaluation Based on Balanced Scorecard with Grey Relational Analysis and Data Envelopment Analysis Approaches: Case Study in Water and Wastewater Companies. *Eval. Program Plan.* **2020**, *79*, 101762. [CrossRef]
17. Yao, Z.; Zhang, T.; Wang, J.; Zhu, L. A Feature Selection Approach Based on Grey Relational Analysis for Within-Project Software Defect Prediction. *J. Grey Syst.* **2019**, *31*, 105–116.
18. Javanmardi, E.; Liu, S.; Xie, N. Exploring Grey Systems Theory-Based Methods and Applications in Sustainability Studies: A Systematic Review Approach. *Sustainability* **2020**, *12*, 4437. [CrossRef]
19. Wang, Y.; Wu, M.; Zhou, Z.; Ma, H. Quantitative Analysis Model of Power Load Influencing Factors Based on Improved Grey Relational Degree. *Power Syst. Technol.* **2017**, *41*, 1772–1778.
20. Biswas, P.; Pramanik, S.; Giri, B.C. Entropy Based Grey Relational Analysis Method for Multi-Attribute Decision Making under Single Valued Neutrosophic Assessments. *Neutrosophic Sets Syst.* **2014**, *2*, 102–110.
21. Wang, Z.; Zhu, H.; Ding, Y.; Zhu, T.; Zhu, N.; Tian, Z. Energy Efficiency Evaluation of Key Energy Consumption Sectors in China Based on a Macro-Evaluating System. *Energy* **2018**, *153*, 65–79. [CrossRef]
22. Olabanji, O.M.; Mpofu, K. Appraisal of Conceptual Designs: Coalescing Fuzzy Analytic Hierarchy Process (F-AHP) and Fuzzy Grey Relational Analysis (F-GRA). *Results Eng.* **2021**, *9*, 100194. [CrossRef]
23. Han, M.; Zhang, R.Q.; Xu, M.L. A Variable Selection Algorithm Based on Improved Grey Relational Analysis. *Control. Decis.* **2017**, *32*, 1647–1652.
24. Vatansever, K.; Akgűl, Y. Performance Evaluation of Websites Using Entropy and Grey Relational Analysis Methods: The Case of Airline Companies. *Decis. Sci. Lett.* **2018**, *7*, 119–130. [CrossRef]
25. Lu, D.; Zhao, X. Day-Ahead Energy Scheduling in Residential Areas Based on Orderly Charge and Discharge of Electric Vehicles. In Proceedings of the 2020 12th IEEE PES Asia-Pacific Power and Energy Engineering Conference (APPEEC), Nanjing, China, 20–23 September 2020; pp. 1–6.
26. Erdinc, O.; Paterakis, N.G.; Mendes, T.D.; Bakirtzis, A.G.; Catalão, J.P. Smart Household Operation Considering Bi-Directional EV and ESS Utilization by Real-Time Pricing-Based DR. *IEEE Trans. Smart Grid* **2014**, *6*, 1281–1291. [CrossRef]
27. Ge, Y.; Shang, C. Energy Storage Planning Constrained by Its Life. *Proc. Proc. CSEE* **2020**, *40*, 6150–6161.
28. Xiang, Y.; Liu, J.; Liu, Y. Robust Energy Management of Microgrid with Uncertain Renewable Generation and Load. *IEEE Trans. Smart Grid* **2015**, *7*, 1034–1043. [CrossRef]
29. Wang, L.Y.; Chen, Q.X.; He, G.N.; Kang, C.Q. Optimization of generation scheduling considering battery energy storage life model. *Autom. Electr. Power Syst.* **2019**, *43*, 93–100.
30. Lu, Z.; Zhao, J.; Tseng, K.J.; Ng, K.W.; Rao, Y. Applying VRB-ESS in the DC Micro-Grid for Green Building Electricity Supply: Constructive Suggestions to Improve the Overall Energy Efficiency. In Proceedings of the 2013 IEEE 10th International Conference on Power Electronics and Drive Systems (PEDS), Kitakyushu, Japan, 22–25 April 2013; pp. 130–135.
31. Shi, Y.; Xu, B.; Wang, D.; Zhang, B. Using Battery Storage for Peak Shaving and Frequency Regulation: Joint Optimization for Superlinear Gains. *IEEE Trans. Power Syst.* **2017**, *33*, 2882–2894. [CrossRef]
32. Hu, H.; Xu, C.; Wu, S.; Ji, J.R. Analysis of factors influencing economy of customer-side distributed generation. *Electr. Autom. Equip.* **2008**, *28*, 29–33.

33. Takami, N.; Inagaki, H.; Tatebayashi, Y.; Saruwatari, H.; Honda, K.; Egusa, S. High-Power and Long-Life Lithium-Ion Batteries Using Lithium Titanium Oxide Anode for Automotive and Stationary Power Applications. *J. Power Sources* **2013**, *244*, 469–475. [CrossRef]
34. Yan, M.; Ai, X.; Zhang, Y.; Shu, K.; Gan, W. Robust Unit Commitment with the Consideration of the Generator Prohibited Zones under the Penetration of Wind Power. *China Soc. for Elec. Eng.* **2018**, *38*, 3195–3203.
35. Xu, N.; Dang, Y.G. Characteristic Adaptive GM (1, 1) Model and Forecasting of Chinese Traffic Pollution Emission. *Syst. Eng.-Theory Pract.* **2018**, *38*, 187–196.
36. Guo, L.; Yang, S.; Liu, Y. Typical Day Selection Method for Capacity Planning of Microgrid with Wind Turbine-Photovoltaic and Energy Storage. *Proc. CSEE* **2020**, *40*, 08.
37. Chicco, G.; Ionel, O.-M.; Porumb, R. Electrical Load Pattern Grouping Based on Centroid Model with Ant Colony Clustering. *IEEE Trans. Power Syst.* **2012**, *28*, 1706–1715. [CrossRef]
38. Ming, D.; Jiaolong, X.; Xinyu, L.; Wenhui, S. The Generation Method and Application of Wind Resources/Load Typical Scenario Set for Evaluation of Wind Power Grid Integration. *Proc. CSEE* **2016**, *36*, 4064–4071.
39. Kuang, Y.; Wang, X.L.; Wang, J.X.; Peng, Q.; Zhao, H.Y.; Wang, X.F. Virtual Power Plant Energy Sharing Mechanism Based on Stackelberg Game. *Power Syst. Technol.* **2020**, *44*, 4556–4564.
40. Qian, S.; Qiu, L. Quantitative study on value of distinguishing coefficient in grey correlation analysis. *Stat. Decis.* **2019**, *10*, 10–14.
41. Lv, F. Research on the identification coefficient of relational grade for grey system. *Syst. Eng.-Theory Pract.* **1997**, *17*, 50–55.